LAWRENCE
LIVERMORE
NATIONAL
LABORATORY

LLNL-JRNL-777491

Nudged elastic band method for solid-solid transition under finite deformation

A. Ghasemi, P. Xiao, W. Gao

June 10, 2019

The Journal of Chemical Physics

Disclaimer

Nudged elastic band method for solid-solid transition under finite deformation

Arman Ghasemi,[1] Penghao Xiao,[2] and Wei Gao[1, a)]

[1)] *Department of Mechanical Engineering, The University of Texas at San Antonio, San Antonio, Texas 78249, United States*

[2)] *Materials Science Division, Lawrence Livermore National Laboratory, Livermore, California 94550, United States*

(Dated: 6 June 2019)

Solid-state nudged elastic band (SSNEB) methods can be used for finding solid-solid transition paths when solids are subjected to constant external stress fields. However, previous SSNEB methods are not appropriate for studying transitions accompanied with finite or large deformation, due to inaccurate evaluation on enthalpy and barrier. In this paper, a finite deformation nudged elastic band (FD-NEB) method is formulated for finding transition paths of solids under finite deformation. Applications of FD-NEB to phase transition of silicon under uniaxial compression from diamond phase to β-tin phase are presented and compared with previous SSNEB method.

[a)] Electronic mail: wei.gao@utsa.edu

I. INTRODUCTION

Nudged Elastic Band (NEB) method is a widely used transition state computational method for finding transition path and barriers. The barriers can be used to calculate chemical reaction or transition rates within the harmonic transition state theory approximation.[1] The transition paths reveal atomic scale mechanisms during transition. Given the initial and final states of a transition process, the NEB computes a minimum energy path (MEP), i.e. the most probable transition path. NEB method has been applied to study a wide range of problems such as materials phase transition,[2,3] dislocation motion,[4,5] fracture,[6] diffusion[7] and so on.

The NEB method was first proposed in the mid-1990s[8,9] and since then there have been a number of improvements. One important improvement is to generalize the method for studying transitions of solid-state materials. Because the conventional NEB only takes atomic positions as transition variables, the lattice geometries are not adjustable in calculation process. Hence, it can not be directly applied to study solid-solid transitions where lattice deformation and external stress field also contribute to the search of MEP. To this end, solid-state NEB methods were proposed to include the influence of lattice deformation. Trinkle *et al.* coupled the conventional NEB with a full relaxation on the lattice cell.[10] By contrast, Caspersen and Cater used NEB exclusively for lattice cell while always maintaining the atoms in relaxed position (a rapid-nuclear-motion approximation).[11] Noticed that these two approaches are only appropriate for the mechanisms either dominated by atomic or lattice changes, Sheppard *et al.* proposed a generalized solid-state nudged elastic band (G-SSNEB) method,[12] which treats the atomic and lattice variables on equal footing so that transitions involving changes in all degrees of freedom are properly described. Similar to the concept of G-SSNEB, Qian *et al.* developed a variable cell nudged elastic band (VC-NEB) method in which force vectors are expanded along the gradient of potential energy surface.[13]

We notice that the above methods proposed for solid-solid transition are limited to infinitesimal or small deformation. When a stressed solid undergoes finite deformation during transition, the barriers evaluated from these methods are not accurate due to the choice of stress and deformation measurements. In this paper, a finite deformation nudged elastic band (FD-NEB) method is proposed based on the concept of G-SSNEB, for determining MEP of solid-state materials under finite deformation. The remainder of the paper is orga-

nized as follows. To provide readers a basic background, we first summarize the principles of NEB and G-SSNEB methods and then discuss the limitations for studying finite deformation. After that, the FD-NEB method is formulated by adding finite deformation variables to the framework of G-SSNEB method. Finally, an example on stress dependent phase transitions of silicon from diamond phase to β-tin phase is used to demonstrate the application of FD-NEB method.

II. NEB/G-SSNEB AND LIMITATIONS

A. NEB method

In NEB calculation, an elastic band is initially constructed by connecting a number of intermediate states which are generated by linear interpolation between the given initial and final states. The purpose of NEB calculation is to move the elastic band until it converges to MEP. For a system containing N atoms, each state on the elastic band has $3N$ degrees of freedom, so the configuration space of each state is described by a $3N$-dimension vector $\boldsymbol{R} = (\boldsymbol{r}_1, \boldsymbol{r}_2, \cdots, \boldsymbol{r}_N)$ where $\boldsymbol{r}$ represents atom positions. Note that none of the intermediate states are in equilibrium, so they are subjected to the *potential forces* coming from the gradient of the potential energy

$$\boldsymbol{f}^i_{\text{pot}} = -\nabla \mathcal{V}(\boldsymbol{R}^i), \tag{1}$$

which is a $3N$-dimension force vector, evaluated directly from atomistic calculations (either through empirical potentials or first principle methods). The superscript i represents i-th state along the elastic band. Just minimizing these forces would of course only move the intermediate states into local energy minima, and thus would not help to find the MEP. Therefore, in order to keep the intermediate states evenly spaced on the elastic band, *spring forces* are applied between adjacent states, which is also a $3N$-dimension force vector. To avoid the sensitivity of selecting spring constant values for convergence, only certain components of forces are used in calculation. Specifically, the *total force* of intermediate state i is

$$\boldsymbol{f}^i = \boldsymbol{f}^i_{\text{pot}}\,|_{\perp} + \boldsymbol{f}^i_{\text{spr}}\,|_{\parallel}, \tag{2}$$

where $\boldsymbol{f}^i_{\text{pot}}\,|_{\perp}$ is the potential force perpendicular to the elastic band and $\boldsymbol{f}^i_{\text{spr}}\,|_{\parallel}$ is the spring force parallel to that. The tangent vector to the elastic band at each state can be

calculated based on the distance between two adjacent states as well as the surrounding energy landscape.[14] The total force calculated by Eq. (2) is used to drive the elastic band to MEP by force-based optimization algorithms.[15] The optimization runs until the total force is reduced to zero. Then, the corresponding transition state (highest saddle point) can be obtained with climbed image method.[16]

B. Solid-state NEB method

The only degrees of freedom in NEB described above are atom positions, so the geometries of computation cell is not adjustable during the search of MEP. Solid-state NEB method generalizes the atom configuration space by adding lattice cell deformation. Consider a crystal lattice subjected to a constant *Cauchy stress* tensor $\boldsymbol{\sigma}_{\text{app}}$. Due to the lattice deformation, an *internal restoring stress* $\boldsymbol{\sigma}^i_{\text{cell}}$ is generated inside the lattice cell, which can be evaluated directly from atomistic calculations. At equilibrium condition, the applied stress $\boldsymbol{\sigma}_{\text{app}}$ equals to the restoring stress $\boldsymbol{\sigma}^i_{\text{cell}}$. However, the intermediate states on elastic band are not in equilibrium during transition process, so $\boldsymbol{\sigma}^i_{\text{cell}} \neq \boldsymbol{\sigma}_{\text{app}}$ on these states. Similar to NEB, springs have to be prescribed between neighboring states. The *resultant spring stress* is represented by $\boldsymbol{\sigma}^i_{\text{spr}}$. Then, the *total stress* acting on the lattice of intermediate state i is

$$\boldsymbol{\sigma}^i = (\boldsymbol{\sigma}_{\text{app}} - \boldsymbol{\sigma}^i_{\text{cell}})\,|_{\perp} + \boldsymbol{\sigma}^i_{\text{spr}}\,|_{\parallel}, \tag{3}$$

where $\perp$ and $\parallel$ represent the components perpendicular and parallel to the elastic band. In G-SSNEB,[12] the spring stress is calculated as

$$\boldsymbol{\sigma}^i_{\text{spr}} = k\left(\bar{\boldsymbol{\epsilon}}^i_{+} - \bar{\boldsymbol{\epsilon}}^i_{-}\right), \tag{4}$$

where k is spring constant (whose magnitude can be taken as the same one for atomic degree of freedom), and $\bar{\boldsymbol{\epsilon}}^i_{+}$ and $\bar{\boldsymbol{\epsilon}}^i_{-}$ are respectively the strains between states i and $i+1$ and between states i and $i-1$. The bar indicates an average on the strains. For instance, $\bar{\boldsymbol{\epsilon}}^i_{+}$ is an average of the forward strain (use state i as a reference) and the backward strain (use state $i+1$ as a reference). The purpose of doing average is to make sure that, when initial and final states are switched, the reaction path calculated by the algorithm is symmetric to the path obtained before the switch. It should be noted that the strain defined in G-SSNEB is different from the conventional strains used in mechanics (see discussions in Section III A).

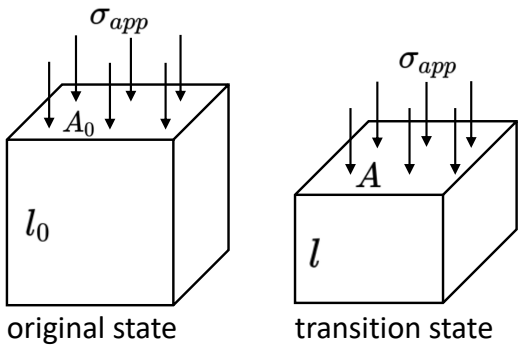

FIG. 1. Schematic of phase transition of a cubic crystal under a constant compressive Cauchy stress.

The atomic and cell variables are treated at equal footing in G-SSNEB. To achieve this, the total stress in Eq. (3) is combined with the total atomic force in Eq. (2) to form a *generalized force vector*, which is then used for optimization. To achieve better convergence, scaling factors are applied to the stresses to ensure their magnitudes scale similarly as the atomic force.[12] The cell geometries and atom positions are simultaneously updated by the total stress $\boldsymbol{\sigma}^i$ and atom force $\boldsymbol{f}^i$ until a MEP is converged. Finally, the transition barrier ($\Pi^{\neq}$) is calculated by the enthalpy difference between initial and transition states

$$\Pi^{\neq}(\boldsymbol{\sigma}_{\text{app}}) = \mathcal{V}^{\neq}(\boldsymbol{\sigma}_{\text{app}}) - V_0 \boldsymbol{\sigma}_{\text{app}} : \boldsymbol{\epsilon}^{(\text{t})}, \tag{5}$$

where $\mathcal{V}^{\neq}$ is the potential energy difference between transition and initial states, V_0 is the volume of initial lattice and $\boldsymbol{\epsilon}^{(\text{t})}$ is the strain tensor at transition state with respect to the initial state.

C. Limitation for finite deformation

In G-SSNEB, stress is measured by Cauchy stress, which is *(force in current state)/(area in current state)* by definition. As a known fact in continuum mechanics, Cauchy stress is not work conjugate to any kind of strain, including the strain defined in G-SSNEB. Therefore, the inner product in Eq. (5) is *ill-defined* and does not yield correct work done by external stress under finite deformation.

This can be simply illustrated by an example shown in Fig. 1, where a cubic crystal undergoes phase transition when it is subjected to a constant compressive Cauchy stress σ_{app}.

Due to Poisson effect, the cross section area increases upon compression, so the applied total force, calculated by $\sigma_{app}A$, also increases during transition. Hence, the work done by this varying force has to be calculated by an integration given the force-displacement relationship (which is usually not a prior knowledge for transition). The work calculated from Eq. (5), denoted by $\sigma_{app}A_0(l - l_0)$, can only serve as an approximation for small deformation when $A \approx A_0$.

Indeed, in a laboratory it is the applied force that is easily controlled, not the Cauchy stress due to the difficulty of tracking the deformed area. Therefore, other types of stress, such as first or second *Piola-Kirchhoff (P-K) stress* (detailed discussion on these stresses is in section III A) are used in mechanics for finite deformation. For example, the *first P-K stress* (also known as *nominal stress*), denoted by a second order tensor $\mathbf{P}$, is the *(force in current state)/(area in reference state)*.[17] Based on this definition, when applied force is a constant, the stress $\mathbf{P}$ also stays as constant. In previous example, if $\mathbf{P}$ is used as a control variable for searching MEP, the work can then be correctly calculated as $P_{app}A_0(l - l_0)$.

There is a special case – *hydrostatic* compression, where Cauchy stress (the pressure p) is a constant, hence P-K stresses are not suitable for SSNEB calculation. In this case, the work is simply $p\Delta V$ where ΔV is the volume change. It is worth to point out that Eq. (5) implemented in G-SSNEB code gives wrong work evaluation for this case. For example, when a cubic with unit length is hydrostatically compressed by a unit pressure into a cubic with half of unit length, the correct work should be 7/8 while Eq. (5) yields 3/2.

It is certainly of interest for G-SSNEB users to examine their previous results, when the barrier values are critical in their studies. First of all, if applied stress is zero, there is no work evaluation so the barrier calculated by G-SSNEB is accurate. When applied stress is not zero, one needs to check the change of the surface area on which the stress is applied. If the change is small and negligible, the barriers calculated by G-SSNEB are acceptable. For example, during a transition under pure shear deformation, if the lattice surface area varies little, G-SSNEB results provide a good approximation even though the lattice shape could be substantially sheared. In addition, as discussed above, the calculations for hydrostatic compression cases with G-SSNEB code also require examination.

When the first or second P-K stress is used for SSNEB calculation, the lattice deformation should be measured with their work conjugate pairs: deformation gradient or Green-Lagrangian strain. It is important to note that the correction cannot be done by only simply

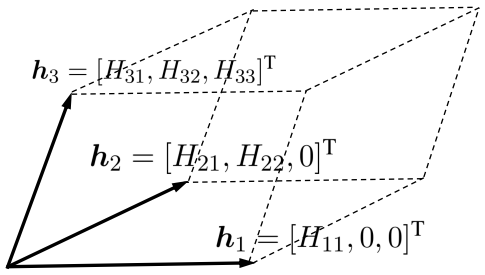

FIG. 2. Schematic of lattice cell used in FD-NEB calculation, defined by 3 lattice vectors.

converting $\boldsymbol{\sigma}_{\mathrm{app}}$ and $\boldsymbol{\epsilon}^{(\mathrm{t})}$ into the stress and strain of the correct types at the evaluation of work, because this does not affect the searching of MEP. Therefore, a different formulation on the computation method is needed.

III. FD-NEB ALGORITHM

A. Description of finite deformation

A crystal can be modeled by a lattice cell that is replicated by periodic boundary conditions along three lattice vectors $\boldsymbol{h}_1$, $\boldsymbol{h}_2$ and $\boldsymbol{h}_3$. Then, the cell geometry can be described by a cell matrix $\mathbf{H} = \begin{bmatrix} \boldsymbol{h}_1 & \boldsymbol{h}_2 & \boldsymbol{h}_3 \end{bmatrix}$. Like G-SSNEB, we can further confine $\boldsymbol{h}_1$ and $\boldsymbol{h}_2$ to axis-1 and plane 1-2, as shown in Fig. 2. In this way, the rotational degrees of freedom of lattice are eliminated and $\mathbf{H}$ only includes 6 independent variables

$$\mathbf{H} = \begin{bmatrix} H_{11} & H_{21} & H_{31} \\ 0 & H_{22} & H_{32} \\ 0 & 0 & H_{33} \end{bmatrix}. \tag{6}$$

The change of the nonzero component H_{ij} can be considered as the kinematics resulted from the corresponding σ_{ij} acting on the cell, which is defined in Eq. (3). This feature has been used in G-SSNEB for stress based cell optimization.

To describe finite deformation, a reference state has to be specified so that deformation and stress can be evaluated based on this state. While there is no restrictions on choosing the reference state, for convinces, we select the *initial state under zero stress* as the reference state in FD-NEB calculations. The lattice vectors and cell matrix of this reference state are represented by $\boldsymbol{h}_\alpha^0 (\alpha = 1, 2, 3)$ and $\mathbf{H}^0$. For an arbitrary state i on the elastic band, the

lattice vectors and cell matrix are represented by $\boldsymbol{h}_\alpha^i$ and $\mathbf{H}^i$. Under a homogeneous finite deformation, $\boldsymbol{h}_\alpha^0$ can be mapped to $\boldsymbol{h}_\alpha^i$ by a second order *deformation gradient* tensor $\mathbf{F}$

$$\boldsymbol{h}_\alpha^i = \mathbf{F}^i \boldsymbol{h}_\alpha^0, \tag{7}$$

where $\mathbf{F}^i$ represents a finite deformation mapping of state i. Using cell matrix, $\mathbf{F}^i$ can be written as

$$\mathbf{F}^i = (\mathbf{H}^i)(\mathbf{H}^0)^{-1}. \tag{8}$$

The work conjugate of $\mathbf{F}$ is the first P-K stresses $\mathbf{P}$, which is related to Cauchy stress by

$$\mathbf{P} = J\boldsymbol{\sigma}\mathbf{F}^{-\mathrm{T}}, \tag{9}$$

where $J = \det\mathbf{F}$ is the Jacobian of deformation gradient. The inner product $V_0\mathbf{P} : (\mathbf{F} - \mathbf{I})$ provides the correct work done by a constant stress $\mathbf{P}$ under finite deformation, where the identity tensor represents undeformed state. Therefore, $\mathbf{F}$ and $\mathbf{P}$ can be taken as control variables in FD-NEB. As discussed in Section II C, one advantage of using $\mathbf{P}$ is that it can be directly controlled and measured from experiments when the applied force is known.

In continuum mechanics[17,18], another commonly used work conjugate pair are *second P-K stress* tensor ($\mathbf{S}$) and *Green-Lagrangian strain* tensor ($\mathbf{E}$), which are defined by

$$\mathbf{S} = J(\mathbf{F})^{-1}\boldsymbol{\sigma}(\mathbf{F})^{-\mathrm{T}}, \tag{10}$$

and

$$\mathbf{E} = \frac{1}{2}\left[(\mathbf{F})^{\mathrm{T}}\mathbf{F} - \mathbf{I}\right]. \tag{11}$$

The second P-K stress is conceptually defined by *(force in reference state)/(area in reference state)*, a tensor entirely defined in reference configuration, so it does not have a direct physical interpretation. However, second P-K stress has mathematical advantages for many theoretical formulations such as describing materials constitutive behavior. Therefore, it may be useful if one wants to integrate FD-NEB calculation to higher level thermodynamic modeling methods in which second P-K stress is needed.

It is noted that, in G-SSNEB, the strain is defined by $\boldsymbol{\epsilon} = \mathbf{H}^{\mathrm{def}}\mathbf{H}^{-1} - \mathbf{I}$, where $\mathbf{H}^{\mathrm{def}}$ is for deformed cell. Therefore, G-SSNEB actually uses deformation gradient ($\mathbf{H}^{\mathrm{def}}\mathbf{H}^{-1}$) instead of conventional strains to measure the deformation.

B. Add P-K stress to MEP search

In FD-NEB, the finite deformation variables defined above are used for searing MEP and computing transition barriers. There are two possible ways to do this. The first way is to convert the restoring stress (obtained from atomistic calculations, so Cauchy stress) into P-K stress, which can be combined with the prescribed P-K stress and spring stress to form a new total P-K stress. Then, the cell optimization can be done with this total P-K stress. Instead of this way, we take another approach which requires minimum modification to G-SSNEB. For each state on elastic band, the prescribed P-K stress is converted to a Cauchy stress based on Eq. (9) or (10). For example, if the first P-K stress is used, the prescribed Cauchy stress on state i is calculated as

$$\boldsymbol{\sigma}^i_{\text{app}} = \frac{1}{J}\mathbf{P}_{\text{app}}(\mathbf{F}^i)^{\text{T}}, \tag{12}$$

where $\mathbf{P}_{\text{app}}$ is the applied first P-K stress. In this way, the cell optimization is always controlled by total Cauchy stress. The same spring stress and scaling factors used in G-SSNEB can be applied here.

After the MEP is obtained based on the modified stress, the transition barrier is calculated as

$$\Pi^{\neq}(\mathbf{P}_{\text{app}}) = \mathcal{V}^{\neq}(\mathbf{P}_{\text{app}}) - V_0\mathbf{P}_{\text{app}} : (\mathbf{F}^{(\text{t})} - \mathbf{F}^{(\text{o})}), \tag{13}$$

where $\mathcal{V}^{\neq}$ is the potential energy difference between transition and initial states, $\mathbf{F}^{(\text{t})}$ and $\mathbf{F}^{(\text{o})}$ are respectively the deformation gradients of transition and initial states under stress $\mathbf{P}_{\text{app}}$ with respect to the reference state (whose volume is V_0). For the second P-K stress, one just needs to replace $\mathbf{P}_{\text{app}}$ and $\mathbf{F}$ in Eq. (13) respectively with $\mathbf{S}_{\text{app}}$ and $\mathbf{E}$.

Before running FD-NEB, the lattice at both initial and final states have to be deformed to target stress $\mathbf{P}_{\text{app}}$ by using any force-based optimization such as damped dynamics algorithm. Similar to what is applied in FD-NEB, $\mathbf{P}_{\text{app}}$ is first converted to $\boldsymbol{\sigma}_{\text{app}}$. Then, the residual stress $\boldsymbol{\sigma} = \boldsymbol{\sigma}_{\text{app}} - \boldsymbol{\sigma}_{\text{cell}}$ can be gradually reduced to zero by adjusting lattice geometries such that the lattice can be optimized to the target stress $\mathbf{P}_{\text{app}}$.

C. Decouple atomic motion

The displacements of the mean positions of atoms in the periodic cell during MEP search conceptually include two parts: (1) the displacements solely in response to lattice defor-

mation; (2) the displacements due to reaction (or transition) regardless of cell motion. As mentioned in the previous work,[12] to avoid double-counting cell motion in MEP search, it is important to decouple the contribution from the first part when calculating the distance between two neighboring states in the atomic configuration space, $\Delta \boldsymbol{R}$, which is used for spring force and tangent direction calculations. In FD-NEB, we implemented a slightly different method from G-SSNEB to decouple atomic motions respectively from cell deformation and reaction.

In previous G-SSNEB, $\Delta \boldsymbol{R}$ is first calculated based on fractional coordinates, which is then covered back to Cartesian coordinates. Based on the definition of fractional coordinates, the Cartesian coordinates of one atom at state i is $\boldsymbol{r}^i = \mathbf{H}^i \boldsymbol{\zeta}^i$, where $\boldsymbol{\zeta}$ denotes fractional coordinates. The displacements of such atom due to the cell motion from state i to $i+1$ can be (only approximately for multilattices) written as

$$\Delta \boldsymbol{r}^i_{\text{cell}} = \left(\mathbf{H}^{i+1} - \mathbf{H}^i\right) \boldsymbol{\zeta}^i. \tag{14}$$

This displacements have to be taken out from the total atom displacements, denoted by $\Delta \boldsymbol{r}^i_{\text{tot}} = \mathbf{H}^{i+1}\boldsymbol{\zeta}^{i+1} - \mathbf{H}^i\boldsymbol{\zeta}^i$. Then the second part of displacements due to reaction is $\Delta \boldsymbol{r}^i_{\text{rec}} = \Delta \boldsymbol{r}^i_{\text{tot}} - \Delta \boldsymbol{r}^i_{\text{cell}}$. However, instead of using this, $\Delta \boldsymbol{r}^i_{\text{rec}}$ in G-SSNEB is calculated by $\left(\boldsymbol{\zeta}^{i+1} - \boldsymbol{\zeta}^i\right) \bar{\mathbf{H}}$, where $\bar{\mathbf{H}} = \left(\mathbf{H}^{i+1} + \mathbf{H}^i\right)/2$ is an averaged cell matrix. Although this provides a reasonable approximation, a more well-defined formulation is implemented in FD-NEB.

Based on the relationship between $\mathbf{H}$ and deformation gradient $\mathbf{F}$ in Eq. (8), Eq. (14) can be also written in terms of $\mathbf{F}$

$$\Delta \boldsymbol{r}^i_{\text{cell}} = \left(\mathbf{F}^{i+1} - \mathbf{F}^i\right) \boldsymbol{r}^0, \tag{15}$$

where $\boldsymbol{r}^0$ is the atom's Cartesian coordinates in reference state. In this way, there is no need to convert between Cartesian and fractional coordinates. Instead, Eq. (15) is directly implemented in FD-NEB. Note that Eq. (15) is indeed a representation of the *Cauchy rule*,[18] which states that atoms behave as material points embedded in the continuum solid, and simply follow the macroscopic deformation exactly.

It should be noted that Cauchy rule has to be corrected for multilattices with *Cauchy-Born rule*,[18,19] which states that atom displacements due to cell deformation include not only the part set by macroscopic deformation gradient but also an *internal relaxation* associated

with the relative motion of sublattices. Mathematically, $\boldsymbol{r} = \mathbf{F}\boldsymbol{r}^0 + \boldsymbol{\eta}$, where $\boldsymbol{\eta}$ is the internal relaxation. $\boldsymbol{\eta}$ is usually obtained from molecular statics calculation with full ion relaxation. How to evaluate and incorporate the influence of $\boldsymbol{\eta}$ in MEP search would be an interesting question for future study. However, in current FD-NEB, the influence of $\boldsymbol{\eta}$ is neglected.

D. Implementation of FD-NEB

FD-NEB is implemented based on the the Atomic Simulation Environment (ASE), an open source Python package which has also been used for G-SSNEB. The advantage of using ASE is that it provides an interface to various external atomistic computational codes, such as VASP and LAMMPS. ASE can create an 'Atom object' that has information of potential energy, atom positions and force, lattice geometries and Cauchy stress. These atomic attributes will be read by FD-NEB for calculating force and stress defined above. Finally, the calculated force and stress will be passed to a force-based optimization algorithm for updating atom positions and lattice vectors. The FD-NEB computation code is developed based on G-SSNEB code. It was implemented based on an open source project Transition State Library for ASE (TSASE).

IV. EXAMPLE: PHASE TRANSITION OF SILICON UNDER STRESS

The phase transition of Silicon (Si) is used to demonstrate the application of FD-NEB for solid-solid transition under external stress field. At ambient conditions, the most stable phase of Si is a diamond structure. Under compressive stress, Si undergoes a first order phase transition from the diamond structure (Si-I) to the metallic β- tin structure (Si-II). With further increase of compression, Si continuously exhibits many other different phases. Releasing loads does not lead to a recover of the initial Si-I phase but instead to a series of metastable phases.[20] Therefore, phase transition of Si is a rather complicated process, and there are still many unknowns despite decades of research on both experimental[21–23] and theoretical[24–27] sides. Particularly, we have not found any transition state calculations on Si to show how external stress changes the phase transition barriers.

Here, we focus on the transition from Si-I to Si-II on a pristine Si structure. Meanwhile, the transition under an uniaxial compression is considered. An important feature of this

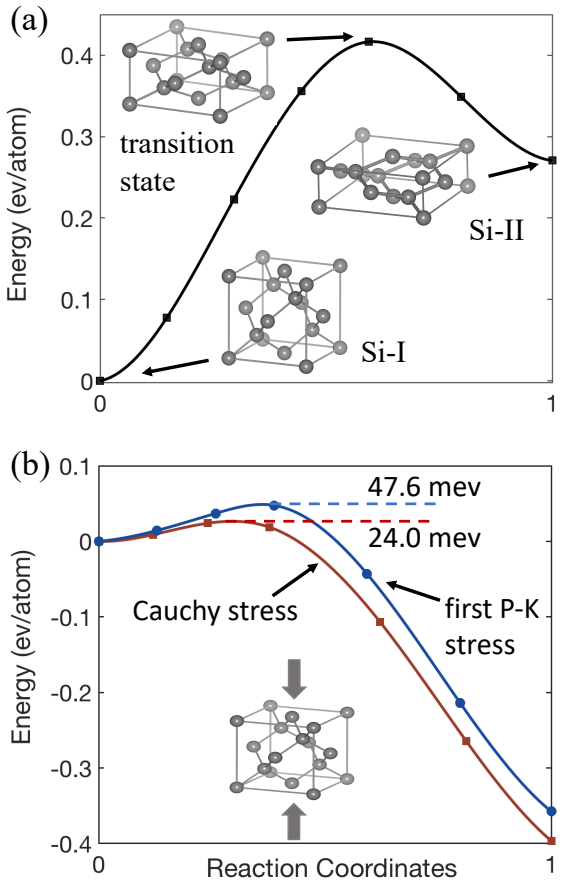

FIG. 3. (a) Zero stress MEP. The inserted images show atomic structures of Si-I (5.47 Å×5.47 Å×5.47 Å), Si-II (6.92 Å×6.92 Å×2.55 Å) and transition state (6.35 Å×6.35 Å×3.45 Å). (b) Comparison of MEPs calculated by using Cauchy stress (with G-SSNEB) and first P-K stress (with FD-NEB) at 10GPa compressive stress. MEPs are fitted with splines.

phase transition is that Si lattice is deformed up to 35% (measured between initial and transition states) and hence a finite deformation problem.

The energy, interatomic force and stress are evaluated by density functional theory (DFT). All the DFT calculations in this study were performed using the plane-wave-based Vienna Ab-initio Simulation Package (VASP[28,29]). Electron exchange and correlation are calculated with the generalized gradient approximation using the Perdew–Burke–Ernzerhof functional (PBE) functional.[30] Projector augmented wave (PAW) pseudopotentials[31,32] were used to represent ionic cores, and the electronic kinetic energy cutoff for the plane-wave basis describing the valence electrons was set to 319 eV. A $6 \times 6 \times 6$ k-point mesh is used to sample Brillouin zone.

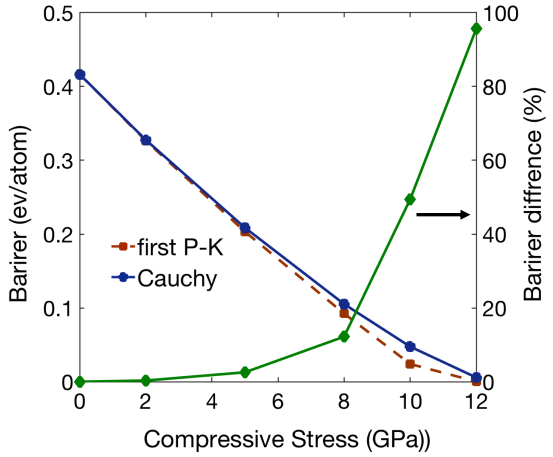

FIG. 4. Barriers as a function of applied stress. The differences are calculated by $(\Pi^{\neq}_{\text{Cauchy}} - \Pi^{\neq}_{\text{PK}})/\Pi^{\neq}_{\text{PK}}$.

The atomic structure of Si used in this study at different phases are shown as the inserted images in Fig. 3. The supercell contains 8 atoms. At zero stress, there is no work evaluation in MEP calculation, so FD-NEB yields the same results as G-SSNEB, as shown in Fig. 3a. We found that the reaction coordinate primarily involves lattice degrees of freedom. When a constant load is applied, the first P-K stress stays as a constant throughout the transition process while the Cauchy stress varies. If one disregards this practical loading constrains, second P-K stress can also be used legitimately. Although Cauchy stress leads to ill-defined and incorrect enthalpy evaluations, the calculations with both Cauchy and P-K stress are conducted at different stress levels for comparison. The typical MEP is shown in Fig. 3b for 10 GPa stress. It is not surprising that different stress representations not only lead to different barriers but also different paths. This difference becomes more significant as the increase of applied stress, demonstrated by the variation of barriers with stress in Fig. 4a. It is noted that the barrier disappears when the applied Cauchy stress is beyond 12 GPa, which means that the transition could occur in this case without any thermal activation.

The transition pathway calculated with Cauchy stress is qualitatively similar to the ones calculated with P-K stress in this example. However, it may not be the case for other material systems. If two or several (stress sensitive) competing transition mechanisms exist simultaneously, the calculation conducted with Cauchy stress may lead to a false pathway due to the incorrect evaluation of enthalpy. Unfortunately, an exemplary material system

has not been identified to show this. Finally, it will be an interesting study by varying total six components of applied stress, not only for phase I and II but also all other possible phases. FD-NEB method developed herein can be a useful and reliable tool for this.

V. SUMMARY

Under external stress, solid-solid transitions are usually accompanied with finite lattice deformation. Accurate evaluation of the transition barriers are critical for computing kinetic rates of the transition. In this paper, we emphasize that previous solid-state NEB algorithm may lead to inaccurate barrier calculations and wrong reaction path, when Cauchy stress is used for work evaluation. The FD-NEB method is formulated by introducing finite deformation variables to G-SSNEB method, and implemented based on facile modifications to previous algorithm. An example of silicon phase transition is presented to demonstrate the difference brought by the new implementation.

ACKNOWLEDGMENTS

W.G. acknowledges the startup fund from University of Texas at San Antonio (UTSA) and the Grant for Research Advancement and Transformation (GREAT) from UTSA Office of the Vice President for Research, Economic Development, and Knowledge Enterprise. Part of P.X.′s work was performed under the auspices of the U.S. Department of Energy by Lawrence Livermore National Laboratory under Contract Number DE-AC52-07NA27344. The authors acknowledge the Texas Advanced Computing Center (TACC) at the University of Texas at Austin for providing HPC resources that have contributed to the research results reported within this paper.

REFERENCES

[1]R. A. Olsen, "An introduction to transition state theory," Winter school lecture at Hansur-Lesse, Belgium (2006).

[2]P. Xiao and G. Henkelman, "Communication: From graphite to diamond: Reaction pathways of the phase transition," The journal of chemical physics **137**, 101101 (2012).

[3]P. Xiao, J.-G. Cheng, J.-S. Zhou, J. B. Goodenough, and G. Henkelman, "Mechanism of the $CaIrO_3$ post-perovskite phase transition under pressure," Physical Review B **88**, 144102 (2013).

[4]T. Zhu, J. Li, A. Samanta, A. Leach, and K. Gall, "Temperature and strain-rate dependence of surface dislocation nucleation," Physical Review Letters **100**, 025502 (2008).

[5]R. Ramachandramoorthy, W. Gao, R. Bernal, and H. Espinosa, "High strain rate tensile testing of silver nanowires: rate-dependent brittle-to-ductile transition," Nano letters **16**, 255–263 (2015).

[6]S. Huang, S. Zhang, T. Belytschko, S. S. Terdalkar, and T. Zhu, "Mechanics of nanocrack: fracture, dislocation emission, and amorphization," Journal of the Mechanics and Physics of Solids **57**, 840–850 (2009).

[7]M. Villarba and H. Jónsson, "Diffusion mechanisms relevant to metal crystal growth: Pt/Pt (111)," Surface science **317**, 15–36 (1994).

[8]H. Jónsson, G. Mills, and K. W. Jacobsen, "Nudged elastic band method for finding minimum energy paths of transitions," in *Classical and quantum dynamics in condensed phase simulations* (World Scientific, 1998) pp. 385–404.

[9]G. Mills, H. Jónsson, and G. K. Schenter, "Reversible work transition state theory: application to dissociative adsorption of hydrogen," Surface Science **324**, 305–337 (1995).

[10]D. Trinkle, R. Hennig, S. Srinivasan, D. Hatch, M. Jones, H. Stokes, R. Albers, and J. Wilkins, "New mechanism for the α to ω martensitic transformation in pure titanium," Physical review letters **91**, 025701 (2003).

[11]K. J. Caspersen and E. A. Carter, "Finding transition states for crystalline solid–solid phase transformations," Proceedings of the National Academy of Sciences **102**, 6738–6743 (2005).

[12]D. Sheppard, P. Xiao, W. Chemelewski, D. D. Johnson, and G. Henkelman, "A generalized solid-state nudged elastic band method," The Journal of chemical physics **136**, 074103 (2012).

[13]G.-R. Qian, X. Dong, X.-F. Zhou, Y. Tian, A. R. Oganov, and H.-T. Wang, "Variable cell nudged elastic band method for studying solid–solid structural phase transitions," Computer Physics Communications **184**, 2111–2118 (2013).

[14]G. Henkelman and H. Jónsson, "Improved tangent estimate in the nudged elastic band method for finding minimum energy paths and saddle points," The Journal of chemical

physics **113**, 9978–9985 (2000).

[15]D. Sheppard, R. Terrell, and G. Henkelman, "Optimization methods for finding minimum energy paths," The Journal of chemical physics **128**, 134106 (2008).

[16]G. Henkelman, B. P. Uberuaga, and H. Jónsson, "A climbing image nudged elastic band method for finding saddle points and minimum energy paths," The Journal of chemical physics **113**, 9901–9904 (2000).

[17]E. B. Tadmor, R. E. Miller, and R. S. Elliott, *Continuum mechanics and thermodynamics: from fundamental concepts to governing equations* (Cambridge University Press, 2012).

[18]E. B. Tadmor and R. E. Miller, *Modeling materials: continuum, atomistic and multiscale techniques* (Cambridge University Press, 2011).

[19]M. Born and K. Huang, *Dynamical theory of crystal lattices* (Clarendon press, 1954).

[20]S. Wippermann, Y. He, M. Vörös, and G. Galli, "Novel silicon phases and nanostructures for solar energy conversion," Applied Physics Reviews **3**, 040807 (2016).

[21]J. Kasper and S. Richards, "The crystal structures of new forms of silicon and germanium," Acta Crystallographica **17**, 752–755 (1964).

[22]J. Z. Hu, L. D. Merkle, C. S. Menoni, and I. L. Spain, "Crystal data for high-pressure phases of silicon," Physical Review B **34**, 4679 (1986).

[23]Y.-X. Zhao, F. Buehler, J. R. Sites, and I. L. Spain, "New metastable phases of silicon," Solid state communications **59**, 679–682 (1986).

[24]A. Mujica, A. Rubio, A. Munoz, and R. Needs, "High-pressure phases of group-iv, iii–v, and ii–vi compounds," Reviews of Modern Physics **75**, 863 (2003).

[25]M. Durandurdu, "Diamond to β-sn phase transition of silicon under hydrostatic and non-hydrostatic compressions," Journal of Physics: Condensed Matter **20**, 325232 (2008).

[26]V. I. Levitas, H. Chen, and L. Xiong, "Triaxial-stress-induced homogeneous hysteresis-free first-order phase transformations with stable intermediate phases," Physical review letters **118**, 025701 (2017).

[27]N. A. Zarkevich, H. Chen, V. I. Levitas, and D. D. Johnson, "Lattice instability during solid-solid structural transformations under a general applied stress tensor: Example of si i $\rightarrow$ si ii with metallization," Physical review letters **121**, 165701 (2018).

[28]G. Kresse and J. Furthmüller, "Efficient iterative schemes for ab initio total-energy calculations using a plane-wave basis set," Physical review B **54**, 11169 (1996).

[29]G. Kresse and J. Hafner, "Ab initio molecular dynamics for liquid metals," Physical Review B **47**, 558 (1993).

[30]J. P. Perdew, K. Burke, and M. Ernzerhof, "Generalized gradient approximation made simple," Physical review letters **77**, 3865 (1996).

[31]G. Kresse and D. Joubert, "From ultrasoft pseudopotentials to the projector augmented-wave method," Physical Review B **59**, 1758 (1999).

[32]P. E. Blöchl, "Projector augmented-wave method," Physical review B **50**, 17953 (1994).